Nonadiabatic and nonlocal electron-phonon interaction and phonon-plasmon mixing in the high-temperature superconductors

Claus Falter and Michael Klenner
Institut für Theoretische Physik II-Festkörperphysik, Universität Münster, Wilhelm-Klemm-Straße 10, 48149 Münster, Germany
(Received 2 May 1994)

Within the framework of an electronic density response approach, recently worked out to describe screening, lattice dynamics, and the electron-phonon interaction in the high-temperature superconductors, it is shown, using La_2CuO_4 as an example, that the already large (nonlocal) electron-phonon coupling as calculated in the adiabatic approximation is further strongly enhanced for certain phonons in the high-temperature superconductors (HTSC's) in the nonadiabatic regime where dynamical screening comes into play. At the same time, a low-lying plasma mode of the electronic system appears for wave vectors in the (0,0,1) direction which mixes strongly with the phonons of appropriate symmetry and leads in addition to the phonons to very large changes of the crystal potential. Such a coexistence of phononlike and plasmonlike modes in the same frequency range is argued to be a specific feature of the HTSC's related to their layered structure and weak screening of the strong ionic forces in the c direction. It leads to a significant increase of the retarded attractive interaction and provides, at least in part, an understanding of the reduction of the oxygen isotope effect in these materials, which is difficult to explain for a pure (harmonic) electron-phonon superconductor.

I. INTRODUCTION

The most important step in order to understand the high T_c values of the cuprate superconductors means to unravel the physical mechanism leading to an increased pair binding. In view of the great success of the electron-phonon interaction (EPI) in explaining superconductivity in the conventional materials it is quite natural to investigate first the EPI in the high-temperature superconductors (HTSC's) and to separate features which are normal (like local EPI effects being the source for superconductivity in the conventional metals) from those which are specific and really important for the HTSC's, and if possible to relate these to the characteristic structural and electronic properties of these compounds. Such attempts have been undertaken, e.g., in Refs. 1–8.

In particular, the calculations in Refs. 2–5, performed within a suitable microscopic model for the electronic density response, indicate that unusual strong nonlocal (long-range) EPI effects appear for certain phonon modes as a consequence of an interplay of the layered crystal structure, the quasi-two-dimensional electronic band structure, and strong ionic forces which are only weakly screened through a mechanism dominated by ionic charge fluctuations. So far these calculations [and of course also all frozen-phonon calculations within density-functional theory (DFT)] have been carried out using the adiabatic approximation, which relies on static screening of the interactions, resulting in short-range forces between quasiparticles (an exception is the calculation leading to the results displayed in Fig. 5 of Ref. 5). As a consequence of this approximation, the important long-range Coulomb correlations which give rise to the (low-lying) plasma modes via dynamical screening and the coupling to the phonons as discussed in this paper are excluded from the beginning.

In Refs. 5 and 8 a nonadiabatic view of electron-phonon coupling has been suggested for high-frequency phonon modes propagating along the $\Lambda\sim(0,0,1)$ direction. In order to simulate qualitatively the reduced screening, as is to be expected in the nonadiabatic regime (see Ref. 5), in Ref. 8 frozen-phonon calculations have been performed in the local-density approximation (LDA) in which electron transfer was locally restricted, leading to a very large electron-phonon coupling.

Static screening, i.e., using the adiabatic approximation for the phonons and ignoring plasmons as further collective excitations of the system within the range of the energy spectrum of the phonons, is in general not a sufficient approximation for certain high-frequency phonon modes along the Λ direction, because there will be mode mixing between these phonons and the low-lying plasmons in the nonadiabatic regime, as our preliminary calculations in Ref. 5 have shown whenever the dispersion of the electronic bands in the c direction is sufficiently small at the Fermi level (and this is likely to be the case; see Refs. 1 and 9). Of course, here it is assumed implicitly that a band picture can be applied in the HTSC's for the c direction. Consequently, an experimental search for the possible existence of the low-lying mixed c-axis phonon-plasmon modes as predicted by our calculations would be helpful in the context of the question concerning the type of electron motion in the c direction, and, in particular, if the above assumption holds or must be supplemented or replaced by some other hopping mechanism in the c direction to lower the kinetic energy in the layered structure of the HTSC's.

Often quoted facts in the literature which are thought not to speak in favor of an EPI-mediated interaction in the HTSC's are the very high T_c values possible in some materials, and the reduced and varying oxygen isotope effect. At least people who can be identified with the EP

community think that the EPI as calculated within the DFT LDA can explain superconductivity for the lower-T_c members of the HTSC's while this may be questionable for the higher-T_c members. On the other hand, the observed isotope effect is hard to explain in a pure (harmonic) EPI picture. Concerning both topics, a nonadiabatic enhancement of the already strong nonlocal, long-ranged EPI effects of ionic origin, as calculated in the adiabatic approximation, together with phonon-plasmon mixing of the special type calculated below may give an answer and may help to solve the HTSC puzzle.

The remainder of the paper is organized in the following way. In Sec. II the theoretical description of the density response and the approximations made are reviewed in a compact form. Section III gives the numerical results and the discussion of the calculated electron-phonon coupling and the coupled phonon-plasmon dispersion. Further, consequences for the oxygen isotope effect are outlined. In Sec. IV the main results are summarized.

II. THEORETICAL METHOD AND MODELING

In this section we review our theoretical method which underlies the treatment of the screening, the lattice dynamics, and the EPI in the HTSC's. More detailed information can be found in our earlier work.[3,5]

We base our calculations concerning the local part of the electronic density response and the EPI, respectively, on a proper ionic model as a reference system. In this model, the crystal energy E, being a function of the configuration $\{\mathbf{R}\}$ of the ions, is given by a sum of pair potentials:

$$E(\{\mathbf{R}\})=E_0+\tfrac{1}{2}\sum_{\mathbf{b},\alpha,\beta}{}'\phi_{\alpha\beta}(|\mathbf{R}^{\mathbf{b}}_{\beta}-\mathbf{R}^{0}_{\alpha}|)\ . \tag{1}$$

The constant energy E_0 comprises the self-energies of the rigid ions. In Eq. (1), $\mathbf{b}$ denotes the unit cells in the crystal, α and β are sublattice indices, and $R^{\mathbf{b}}_{\beta}=\mathbf{R}^{\mathbf{b}}+\mathbf{R}^{\beta}$. The pair potentials $\phi_{\alpha\beta}$ (that depend on the distance of the ions only) are calculated by the method of Gordon and Kim.[10] Using in this method spherical ionic densities, as we do, leads to central forces between the ions. Concerning the ionic charges we take the nominal charges (La^{3+},Cu^{2+},O^{2-}) which appears to be reasonable, though it is by no means necessary. Actually, the (partly) covalent character of Cu-O bonding suggests to apply somewhat decreased charges.[5] The unstable O^{2-} ion is treated with the help of the Watson-sphere method[11] and the ionic densities are calculated with a modified version of the Herman-Skillman program[12] including in particular averaged self-interaction corrections.[13]

The long-range Coulomb part is split off from the pair potentials and is treated exactly using the Ewald method. The remaining short-range part, $\tilde{\phi}$, is calculated numerically on a mesh of ion distances R, and is fitted by the generalized Born-Mayer-type form

$$\tilde{\phi}(R)=\alpha_+ e^{-\beta_+ R}-\alpha_- e^{-\beta_- R}\ . \tag{2}$$

The crystal energy from Eq. (1) is then minimized with respect to the structural parameters, yielding the equilibrium structure for the subsequent phonon calculations. The dynamical matrix is set up using the Ewald method for the long-range Coulomb contribution to the pair potentials and employing Eq. (2) for the short-range interactions.

So far the local part of the electronic density response has been accounted for by the ionic model. Beyond this approximation we additionally include long-range, nonlocal contributions to the density response in the form of electronic charge fluctuations (CF's) on the ions. In a physical picture, one can imagine that electrons are added to or are taken away from the copper d and oxygen p shells of the overlapping ions making up the crystal. Thus, density changes having the shape of the corresponding orbital densities will result. Formally we can account for this change in density by parametrizing the electron density as follows:

$$\rho=\rho(\mathbf{R},\zeta)\ . \tag{3}$$

Here $\mathbf{R}$ is a shorthand notation for the locations of the nuclei $\{\mathbf{R}^{\mathbf{a}}_{\alpha}\}$ and denotes an explicit dependence of ρ on the coordinates of the nuclei. In the present case this comprises the density change corresponding to the rigid displacement of the ionic densities with the nuclei, which just constitutes the rigid-ion model (RIM). The second argument $\zeta=\{\zeta^{\mathbf{b}}_{\kappa}\}$ denotes a set of "generalized coordinates" corresponding to some appropriate degrees of freedom of the density, as, for example, here CF's, the changes of which are not explicitly prescribed with respect to the motion of the nuclei, but are to be determined implicitly from the variational principle of the energy. $\mathbf{b}$ denotes the unit cell the effective electronic degree of freedom (EDF) $\zeta^{\mathbf{b}}_{\kappa}$ is associated with, and κ numbers the different EDF's within the unit cell. According to Eq. (3), the displacement-induced change in density, $\mathbf{P}^{\mathbf{a}}_{\alpha}(\mathbf{r})$,[14] is given by

$$\begin{aligned}\mathbf{P}^{\mathbf{a}}_{\alpha}(\mathbf{r})&=\left[\frac{\partial\rho(\mathbf{r})}{\partial\mathbf{R}^{\mathbf{a}}_{\alpha}}\right]_{\mathrm{tot}}\\&=\left[\frac{\partial\rho(\mathbf{r})}{\partial\mathbf{R}^{\mathbf{a}}_{\alpha}}\right]_{\mathrm{ex}}+\sum_{\mathbf{b}\kappa}\left[\frac{\partial\rho(\mathbf{r})}{\partial\zeta^{\mathbf{b}}_{\kappa}}\right]\frac{\partial\zeta^{\mathbf{b}}_{\kappa}}{\partial\mathbf{R}^{\mathbf{a}}_{\alpha}}\\&\equiv[\mathbf{P}^{\mathbf{a}}_{\alpha}(\mathbf{r})]_{\mathrm{RIM}}-\sum_{\mathbf{b}\kappa}\rho_{\kappa}(\mathbf{r}-\mathbf{R}^{\mathbf{b}}_{\kappa})\mathbf{X}^{\mathbf{ba}}_{\kappa\alpha}\ .\end{aligned} \tag{4}$$

$[\mathbf{P}^{\mathbf{a}}_{\alpha}(\mathbf{r})]_{\mathrm{RIM}}$ gives the explicit change in density associated with the RIM. The densities $\rho_{\kappa}(\mathbf{r})$ describe the shape of the change in density associated with the EDF's and are denoted as form factors. As mentioned above, we identify the form factors with the copper d and oxygen p orbital density in our model. The quantity X that expresses the reaction of the EDF in response to an ion displacement is given, in compact notation, by

$$X=C^{-1}B\ . \tag{5}$$

The coefficients $C^{\mathbf{ab}}_{\kappa\kappa'}$ describe the mutual interaction between the EDF's. They are defined by

$$C^{\mathbf{ab}}_{\kappa\kappa'}=\frac{\partial^2 E(\zeta,R)}{\partial\zeta^{\mathbf{a}}_{\kappa}\partial\zeta^{\mathbf{b}}_{\kappa'}}\ , \tag{6}$$

where $E(\zeta,R)$ is the function which results if Eq. (3) is inserted into the Hohenberg-Kohn energy functional. The quantities $B_i^{\mathbf{b}\kappa\,\mathbf{A}}(\,\mathbf{A}\equiv\mathbf{a}\alpha)$ express the interaction between the EDF and the ions, according to their definition

$$B_i^{\mathbf{b}\kappa\,\mathbf{A}}=\frac{\partial^2 E(\zeta,R)}{\partial\zeta^{\mathbf{b}}_{\kappa}\partial R_i^{\mathbf{A}}}\ . \tag{7}$$

A parametrization of the electron density as in Eq. (3) is obtained in our model by making the ionic charges variable, i.e., $\zeta=\{Z^{\mathbf{a}}_{\alpha}\}$, where $Z^{\mathbf{a}}_{\alpha}$ is the ionic charge of the $\mathbf{a}\alpha$ ion. Likewise as in the ionic model it is supposed that the total electron density of the crystal is given by the superposition of the individual ionic electron densities, where the charge of the latter may now vary in response to the displacements of the ions in a lattice vibration. In this way the rigid-ion Coulomb energy as calculated in the RIM can relax in accordance with the kinetic-energy contribution to C. The energy of the system in the pair-potential approximation, Eq. (1), then depends on the ionic charges, and we may, in principle, calculate the quantities C and B according to Eqs. (6) and (7), respectively, from Eq. (1). Note that also the ionic self-energies have to be considered because they also depend on the ionic charges. In practice, the kinetic-energy contribution is excluded from the pair potentials and the ionic self-energies in calculating the interaction C and is treated in a different manner (see below and Refs. 3 and 5). In varying the ionic charges we ignore relaxation effects, i.e., we do not recalculate self-consistently the ionic wave functions for each value of Z, but do simply put electrons in or out from the fixed outmost shell. The form factors representing the shape of the density variation are then given by the orbital densities of the corresponding shells at the copper and the oxygen ions.

It is convenient to write Eq. (5) in a form known from usual density response theory:[3,5]

$$X=\Pi\varepsilon^{-1}B \tag{8}$$

with

$$\varepsilon=1+\tilde{V}\Pi\ . \tag{9}$$

In Eq. (8) and (9) we have introduced the dielectric function ε and the polarizability Π of the electronic system, describing the kinetic-energy contribution to C. The Coulomb and exchange-correlation (XC) contributions, on the other hand, are contained in the effective electron-electron interaction $\tilde{V}$, which is defined analogously to C in Eq. (6), but with E replaced by its Hartree and XC part only. This separation is useful if we want to discriminate between the screening properties of a metal and those of an insulator, the differences being contained in Π,[3,5] or if we want to extend our model approximatively to the nonadiabatic regime, including dynamical screening.

In the adiabatic approximation within DFT $\Pi^{-1}(\mathbf{r},\mathbf{r}')$ is given by the second functional derivative with respect to the density ρ of the kinetic single-particle energy, and can be represented in a tight-binding approach[3,5] as

$$\Pi_{\kappa\kappa'}(\mathbf{q})=-\frac{2}{N}\sum_{\substack{n,n'\\ \mathbf{k}}}\frac{f_n(\mathbf{k})-f_{n'}(\mathbf{k}+\mathbf{q})}{E_n(\mathbf{k})-E_{n'}(\mathbf{k}+\mathbf{q})}\times[C^*_{\kappa n}(\mathbf{k})C_{\kappa n'}(\mathbf{k}+\mathbf{q})]\times[C^*_{\kappa' n}(\mathbf{k})C_{\kappa' n'}(\mathbf{k}+\mathbf{q})]^*\ . \tag{10}$$

The f's, E's, and C's represent occupation numbers, the electronic band structure, and the expansion coefficients of the Bloch functions in terms of tight-binding functions. N is the number of unit cells in the crystal and κ,κ' are orbital indices. $\mathbf{k}$ and $\mathbf{q}$ denote wave vectors from the first Brillouin zone. The generalization to the nonadiabatic regime (dynamical screening) needed can be achieved by calculating the electronic density response at the frequency ω of the perturbation, i.e., in our case at the phonon frequency. Neglecting in Π the renormalization effects on the quasiparticles introduced by the EPI and also by the low-energy plasmons themselves, dynamical screening can be accounted for by adding $-(\hbar\omega+i\delta)$ to the differences of the single-particle energies in the denominator of the expression for Π in Eq. (10) (note that both scattering channels can lead to a temperature-dependent quasiparticle damping in general, which might have influence on the phonons and plasmons themselves and also on the transport and optical properties in the HTSC's). δ is an infinitesimal small positive real number. In this way the electronic polarizability and thus the electronic density response represented by Eqs. (8) and (9) becomes frequency dependent.

The quantity $\tilde{V}^{\mathbf{ab}}_{\kappa\kappa'}$ in Eq. (9) describes the Coulomb and XC interaction energy of a pair of CF's excited at $\mathbf{a}\kappa$ and $\mathbf{b}\kappa'$. Its intersite contribution is dominated by the long-range Coulomb interaction. The on-site contribution $\tilde{V}^{\mathbf{aa}}_{\kappa\kappa}\equiv U_{\kappa}$ is repulsive and counteracts the occurrence of CF's. It is mainly due to the Coulomb energy associated with the CF form factor densities. In particular, the on-site repulsion for Cu is very large, affecting (besides Π) to a great extent the magnitude of the CF's. Finally, the quantity $B_i^{\mathbf{b}\kappa\,\mathbf{A}}$ describes the change in potential at the $\mathbf{b}\kappa$ CF site when an ion $\mathbf{A}$ is displaced in the i direction. More precisely, it is the change in the potential averaged over the $\mathbf{b}\kappa$ CF form factor. Thus, $B_i^{\mathbf{b}\kappa\,\mathbf{A}}$ gives the driving force for the $\mathbf{b}\kappa$ CF due to a unit displacement of the ion $\mathbf{A}$. $\varepsilon^{-1}B$ then is the screened change of the site potentials in response to a unit displacement. The dominant contribution to B comes from the long-range Coulomb interaction. Note that the potential changes described by B include, in addition to the usual Kohn-Sham potential, a kinetic-energy contribution as well.

For the calculation of $\Pi_{\kappa\kappa'}(\mathbf{q},\omega)$ for La_2CuO_4 we use an eleven-band tight-binding model for the CuO plane, including all the Cu d and $O_{x,y}$ p orbitals.[3,5] In the subsequent steps for the calculation of the density response [Eqs. (8) and (9)] we do not discriminate between the different polarizations (partner functions) of the d or p orbitals, respectively. In particular, we use the same on-site (Coulomb and exchange-correlation) interaction parameters for all pairs of orbitals of an atom, irrespective of polarization. Similarly, also the intersite interaction parameters and the charge-fluctuation–ion interaction parameters (B) are used polarization independent. In this case it

can be shown that working with the full 11×11 polarizability matrix is equivalent to using a "contracted" matrix of size 3×3 that is obtained from the 11×11 matrix by summing over the different polarizations of the Cu d and $O_{x,y}$ p orbitals, respectively. This procedure is different from our previous work[3,5] (an exception is the calculation leading to the results displayed in Fig. 5 of Ref. 5), where we kept only the Cu $d_{x^2-y^2}$ and the O_x,O_y p-σ orbitals in the polarizability matrix, neglecting all the other elements.

In order to introduce interlayer coupling into our calculations, we extend the original two-dimensional tight-binding model by coupling the Cu d orbitals in one layer to the nearest $O_{x,y}$ p orbitals in the two adjacent layers. In this way a (slight) dispersion in the c direction is introduced into the model. The corresponding tight-binding parameters then can be varied in order to study different situations for mixing of the phonon and plasmon degrees of freedom by changing the dispersion of the electronic band structure in the c direction via the interlayer parameters. Altogether, the model seems realistic enough to exhibit the main phenomena introduced by dynamical screening and interlayer coupling.

The coupled-mode frequencies of the phonons and plasmons then must be determined self-consistently from the secular equation for the dynamical matrix which contains ω implicitly via the density response [quantity X in Eq. (8)]. As a further quantity, calculated numerically in Sec. III, which measures directly the strength of the EPI in a certain mode we introduce the self-consistent change of the crystal potential $\delta V_{\rm eff}(\mathbf{q}\sigma,\omega_\sigma(\mathbf{q}),\mathbf{r})$ induced by the phonon mode $\mathbf{q}\sigma$ (σ is the polarization index) at the frequency $\omega_\sigma(\mathbf{q})$ and weighted with the density form factor $\rho_\kappa(\mathbf{r}-\mathbf{R}^\kappa)$ of the electronic charge fluctuation of the ion localized at $\mathbf{R}^\kappa$ in the crystal, i.e.,

$$\delta V_\kappa(\mathbf{q}\sigma,\omega_\sigma(\mathbf{q})) = \int dV \rho_\kappa(\mathbf{r}-\mathbf{R}^\kappa)\delta V_{\rm eff}(\mathbf{q}\sigma,\omega_\sigma(\mathbf{q}),\mathbf{r}) , \quad (11)$$

which can also be expressed in the form (leaving aside a contribution from the kinetic-energy part to B)

$$\delta\phi_\kappa(\mathbf{q}\sigma,\omega_\sigma(\mathbf{q})) = \sum_{\substack{\alpha i \\ \kappa'}} \left[\frac{\hbar}{2M_\alpha\omega_\sigma(\mathbf{q})}\right]^{1/2} e_i^\alpha(\mathbf{q},\sigma) \times\varepsilon^{-1}(\mathbf{q},\omega_\sigma(\mathbf{q}))_{\kappa\kappa'}B_i^{\kappa'\alpha}(\mathbf{q})e^{i\mathbf{q}\cdot\mathbf{R}^\kappa} . \quad (12)$$

The kinetic-energy contribution to B in our model has the same value in the adiabatic and nonadiabatic cases, respectively, and plays no role in the context of the discussion of the strong increase of δV_κ in the nonadiabatic regime as compared to the adiabatic calculation. M_α is the mass of the ion of type α, $\mathbf{e}^\alpha(\mathbf{q},\sigma)$ is the eigenvector of the mode $(\mathbf{q}\sigma)$, $\varepsilon^{-1}_{\kappa\kappa'}$ is the inverse dielectric matrix, implicitly defined by Eqs. (8) and (9), and $B_i^{\kappa'\alpha}(\mathbf{q})$ is the Fourier transform of the quantities $B_i^{\kappa' \mathbf{A}}$.

III. NUMERICAL RESULTS AND DISCUSSION

In this section we present the numerical results for the strong increase of the electron-phonon coupling strength in the nonadiabatic regime. Then we discuss phonon-plasmon mixing along the Λ direction and its dependence on the magnitude of the dispersion of the electronic band structure in the c direction. We also study the conditions for the occurrence of an acoustic plasmon at the Z point and its mixing with the phonons and how this situation changes when interlayer coupling is admitted. Finally, consequences for the oxygen isotope effect in the HTSC's introduced by phonon-plasmon coupling are outlined.

In the context of the nonlocal EPI, we have discussed the very important role of the symmetrical apical oxygen breathing mode at the Z point (O_z^z) in La_2CuO_4,[2,3,5] and also certain oxygen modes at Γ and Z in $YBa_2Cu_3O_7$,[4] polarized along the c direction and inducing favorable charge fluctuation patterns and corresponding changes of the crystal potential in the CuO planes which are important for pairing. Furthermore, an interplay of nonlocal EPI, retardation, and strong Coulomb correlation has provided an interpretation of a universal relationship between T_c and the hole content in the HTSC's.[5] Concerning the O_z^z mode it should be further remarked that it is the highest Λ_1 phonon branch in the RIM (uncoupled phonon mode, dash-dotted curve in Fig. 1) with O_z^z at Z and the LO ferroelectric mode $A_{2u}^{\rm LO}$ (ferro) at Γ which couples strongly to the low-lying plasma mode along the Λ direction (dashed curve in Fig. 1) if the latter is in the region of the O_z^z frequency.

From Table I we can extract the strong increase of the phonon-induced change in the crystal potential $\delta\phi_\kappa$ in the case of O_z^z when passing over from the adiabatic to the nonadiabatic description, taking dynamical screening into account. Besides the results for $\delta\phi_\kappa$ according to Eq. (12), we also have listed in the table the quantity $(\delta\phi_\kappa)^2$ normalized with respect to $(\hbar/2M\omega)$, M being the total mass in the unit cell, in order to facilitate a comparison with other estimates of the coupling, if available. Concerning the absolute values given in Table I, they are probably too large because screening might be underestimated in the present model, in particulate because CF's at O_z and (presumedly less important) at La are neglected. However, the strong increase of the coupling in the nonadiabatic case is a real and very important effect. Looking, for example, at the results for the phononlike mode (Ph) of the nonadiabatic calculation, we realize, based on the large changes of the crystal potential, that screening is drastically reduced in the nonadiabatic treatment of the phonons. In this case the change of the Coulomb interaction which arises in moving the O_z ion remains practically unscreened and leads to the strong increase of $\delta\phi_\kappa$, especially at the Cu site (being shorter in distance), while in the adiabatic calculation these changes of the potential are screened more effectively (but are still large, at least at the oxygen site; see the entries "Ad" and "Adc" in Table I).

Thus the already large coupling strengths which are found in the adiabatic approximation, as in our model or in a density-functional calculation,[6] because of the strong ionic forces, are further enhanced significantly by the nonadiabatic effects, pointing a way for an understanding of high T_c values. Concerning these results and also the appearance of phonon-plasmon mixing considered below,

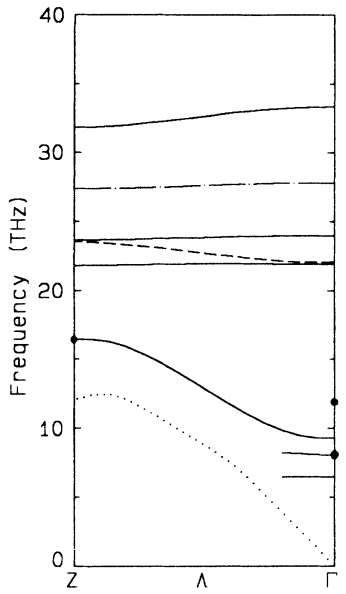

FIG. 1. Calculated phonon (plasmon) dispersion of La_2CuO_4 along the $\Lambda \sim (0,0,1)$ direction for model 1. —— Λ_1-symmetry modes of the coupled system; —·—·— uncoupled phonon; — — — uncoupled plasmon; ··· borderline for damping.

we do not expect that the numerical values are yet accurate enough for quantitative agreement with experiments; however, the basic physical effects exhibited by our calculations should be qualitatively described in a correct way at the level of the present model. In more detail this means a strong increase of δV_κ in the nonadiabatic regime as compared with the adiabatic regime, the existence of a low-lying plasmon mode in the Λ direction strongly coupling with certain phonons of the same symmetry, and a δV_κ for the plasmonlike mode which is even larger than for the phononlike mode. In future work we intend to address these topics more quantitatively by implementing for the electronic band structure a complete tight-binding representation of the corresponding linearized augmented plane wave LDA calculation.

TABLE I. Magnitude of the phonon-induced potential $\delta\phi_\kappa$ in meV (first line of each entry Ad, Ph, Pl, respectively) for La_2CuO_4 at Cu and $O_{x,y}$ in the CuO plane, according to Eq. (12), for the O_z^z mode. The second line of each entry gives for O_z^z $(\delta\phi_\kappa)^2$ normalized by $(\hbar/2M\omega)$ in units of $[(\mathrm{eV/a.u.})^2]$. The values indicated by Ad correspond to (metallic) La_2CuO_4 in the adiabatic approximation. The data in the next two entries correspond to the coupled modes of the nonadiabatic calculation for model 1; see also Fig. 1. The phononlike mode is indicated by Ph and the plasmonlike mode by Pl. The last entry (Adc) in the table gives the results for the complete calculation (δV_κ) in the adiabatic approximation. In contrast to the first three entries Ad, Ph, Pl the results given in this last entry have been corrected for the contribution from the kinetic-energy part of B in order to estimate the influence of the latter.

O_z^z	Cu	O_x	O_y
Ad	8.02	103.00	103.00
	0.32	51.99	51.99
Ph	595.14	376.41	376.41
	1309.45	523.81	523.81
Pl	1135.65	1004.72	1004.72
	9220.30	7216.82	7216.82
Adc	25.91	93.20	93.20
	3.29	42.57	42.57

Next we present our results for the phonon-plasmon mixing in the HTSC's, taking La_2CuO_4 as an example. In Ref. 5 some preliminary remarks on the phonon-plasmon coupling in the HTSC's have been presented as a note added in proof. The main statements can now be substantiated by the numerical data displayed in Figs. 1 and 2 and Table I. The free plasma mode, which has been calculated from the condition $\det\varepsilon = 0$ is given by the dashed line in Figs. 1 and 2. As mentioned above it will couple along the Λ direction (mainly) to A_{2u}^{LO} (ferro) at Γ and, depending on its frequency, to O_z^z or/and La_z^z at the Z point. Note that O_z^z and La_z^z are end points of Λ_1-symmetry branches.

In Figs. 1 and 2 we have shown the branches of Λ_1 symmetry (full lines). In the adiabatic approximation there are six Λ_1 branches[3,5] while in the nonadiabatic coupled-mode treatment as given here an additional plasmonlike branch appears. Note, however, that we have displayed in Figs. 1 and 2 only the undamped solutions where the damping region lies below the dotted curves. In the model corresponding to Fig. 1, model 1 (M1) the lowest (acoustic) Λ_1 branch falls completely into the damping region and so it was omitted. Also the two lowest optical branches in Fig. 1 and the lowest branch in Fig. 2 (model 2) are incomplete because in our calculations we intend to avoid the damping region.

For M1 we assumed a larger dispersion of the electronic band structure in the c direction than for M2. However, the electronic structure is still nearly two dimensional in M1, which should be appropriate to the situation in

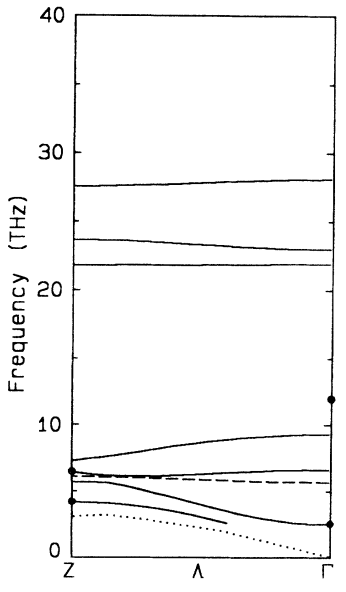

FIG. 2. Same as Fig. 1 (except for the uncoupled phonon which is not shown) but for model 2 as explained in the text.

the HTSC's. The maximal bandwidth in the c direction is about 50 meV at the Fermi level, in accordance with typical results given in Ref. 9. For M1 the plasmonlike extra branch is higher than the phononlike branch. The former is the highest branch in the spectrum shown in Fig. 1. The shape of the phononlike branch is a bit more complicated because mode mixing occurs with another Λ_1 phonon branch lying partly in the damping region. The phononlike branch starts at Γ with A_{2u}^{LO} (ferro) (lower dot) and terminates at Z with O_z^z dot at the Z point).

In M2, which was chosen in order to study the behavior when approaching the two-dimensional limit, the width of the dispersion in the c direction is assumed about a factor of 3 smaller than in M1. Now the situation has changed; the plasmonlike mode is lower than the phononlike mode because the phonons contribute in this case substantially to the screening of the plasma oscillations. At Γ the phononlike branch terminates at A_{2u}^{LO} (ferro) the highest frequency in the spectrum in Fig. 2, while at Z it terminates at La_z^z (upper dot). The plasmonlike branch is modified by mode mixing with another Λ_1 phonon branch. The branch starts at the plasmonlike A_{2u}^{LO} (ferro) mode at Γ (lower dot) and terminates at the plasmonlike La_z^z mode (lower dot at the Z point).

On the other hand, if we increase the dispersion in the c direction in our model sufficiently, we approach the adiabatic regime and the phononlike mode in Fig. 1 turns into its adiabatic shape [branch with the steep dispersion in Fig. 5(b) of Ref. 5]. At the same time the ferroelectric split between A_{2u}^{LO} (ferro) and A_{2u}^{TO} (ferro) (upper dot in Figs. 1 and 2 at Γ) is closed from below. Note in this context that within a certain tube along the Λ direction whose radius depends on ω and increases with decreasing dispersion of the electronic band structure in the (k_x,k_y) plane, the charge response at a given frequency is nonadiabatic (insulatorlike) when the k_z dispersion is sufficiently small. It is only outside this tube that we have a conventional metallic (adiabatic) charge response; compare with the discussion in Ref. 5. Within the tube the plasmon frequencies and the phonon frequencies are of the same order if $q_z \gg q_{x,y}$, i.e., for a conelike region around the Λ direction. In this volume of $\mathbf{q}$ space we have phonon-plasmon mixing and the strong nonadiabatic increase of δV_κ, considered in this work, which are favorable for superconductivity. Remember that we have contributions δV_κ from both the phononlike and the plasmonlike modes. Simultaneously there is a strong enhancement of the phase space for scattering for $\mathbf{q}$ vectors around the Λ direction because of the quasi-two-dimensionality of the band structure,[6] amplifying the importance for pairing via phonon-plasmon scattering. For such a reasoning to apply the usual assumption in context with superconductivity is made that scattering processes within a small energy shell around the Fermi energy are most important.

In the opposite limit, approaching a strictly two-dimensional electronic band structure, i.e., if departures of the Fermi surface from two-dimensionality are neglected, the plasmonlike branch has zero frequency along the Λ direction and the phononlike branch turns into a branch that is characteristic for a two-dimensional insulator; see Fig. 5(a) in Ref. 5. In this limit, when proceeding from the Z point to the (q_x,q_y) plane an acoustic plasmon mode arises [see Fig. 3(a)], where we have calculated the acoustic plasmon along the $\mathbf{q}=(q_x,0,q_z)$ directions for different q_z values. We recognize that the lowest branch belongs to $q_z=2\pi/c$ (Z point) corresponding to an out-of-phase motion of the electrons in different planes. Qualitatively the same CF picture arises in connection with the O_z^z phonon in the metallic phase.[3,5] Figure 3(b) contains besides the uncoupled acoustic plasmon (broken curve) the results for the coupled La_z^z-O_z^z phonon–(acoustic)-plasmon modes near the Z point at $\mathbf{q}=(q_x,0,2\pi/c)$. We observe that mixing occurs in a relative small $\mathbf{q}$-space region around the Λ direction which increases with decreasing dispersion of the electronic band structure in the plane. In context with the acoustic plasmon the work in Ref. 15 should be mentioned. In this paper the possibility of an enhanced plasmon-induced electron pairing is discussed as a possible source for high-T_c superconductivity.

On the other hand, from our discussion above we conclude that in case interlayer hopping is taken into account the plasmon mode at Z is not acoustic but starts at a finite frequency (compare with Fig. 1), and this mode [broken curve in Fig. 3(c)] then replaces the acoustic plasmon [broken curve in Fig. 3(b)] of the strictly two-dimensional situation. Figure 3(c) also contains the mixed phonon-plasmon modes (full curves).

A remark concerning the position of the massive plasmon in other HTSC's which can have additional Fermi-surface (FS) pieces might be appropriate. This position is in general not determined primarily by the largest dispersion of the electronic band structure in the c direction at the Fermi level, but essentially by a weighted average of the dispersion on the Fermi surface. Thus, as long as (possibly) more three-dimensional parts of the FS do not have too much weight, we expect again low-lying plasmon modes in this more complex situation.

In case there is a quasi-two-dimensional van Hove–like peak in the density of states (DOS) $Z(\varepsilon)$ as found in band-structure calculations near the Fermi energy, e.g., caused by a saddle point at a certain $\mathbf{k}$ vector, we have a large contribution to $\Pi(\mathbf{q})$ in the Λ direction in Eq. (10) from this $\mathbf{k}$-space region. Thus the corresponding k_z dispersion of the electronic band structure around this point is very crucial in determining $\Pi(\Lambda)$ in case ε_F is shifted to the peak in the DOS with doping. In this way states around a van Hove–like DOS peak, besides dominating in pairing, additionally have considerable influence on the position of the plasma mode in the Λ direction and consequently on a possible phonon-plasmon resonance. So a correlation between the variation in $Z(\varepsilon_F)$ with doping and the position of the plasma mode can be established. Ultimately, because of the large anisotropy due to the layered structure of the HTSC's consisting of carrier-rich CuO planes alternating with ionic planes with fewer carriers, we have both a relatively high DOS (depending on doping) and simultaneously a strong electron-phonon-plasmon coupling in the same frequency range resulting from nonadiabatic and nonlocal effects, which generates a favorable situation for high-T_c superconductivity.

Considering the aspect of the strong coupling of the electrons to optical phonons like the ferroelectric mode at the Γ point, this situation is similar to the case of polar semiconductors or doped (pseudo)ferroelectrics like $SrTiO_3$. Here at long wavelengths we also obtain mixing of the optical phonon modes and the plasma modes and the electrons then interact via the coupled phonon-plasmon modes. As shown in Refs. 16 and 17, this provides an effective mechanism for pair binding and superconductivity in these materials. By changing the carrier density the resonance frequency of the plasmon can be varied; the same effect can be achieved in the HTSC's by differences in the dispersion of the electronic band structure in the c direction considering different materials or, as discussed above, with doping [possibly leading to variations between the two-dimensional limit and more (anisotropic) three-dimensional behavior] in order to obtain eventually an optimal situation for pair binding, e.g., by shifting the resonance frequencies of the phononlike and plasmonlike branches closer together, thereby optimizing the attractive interaction between the electrons (holes) in the corresponding frequency range. Compare also with the discussion in Ref. 16 where it is argued that the transition temperature is greatly enhanced in case the resonances occur near each other.

A final remark is concerned with applying our findings to the oxygen isotope effect. The strong mode coupling of the plasmon in particular with the axial symmetric apex oxygen breathing mode O_z^z leads to a reduction of this effect in proportion to the plasmon character of this

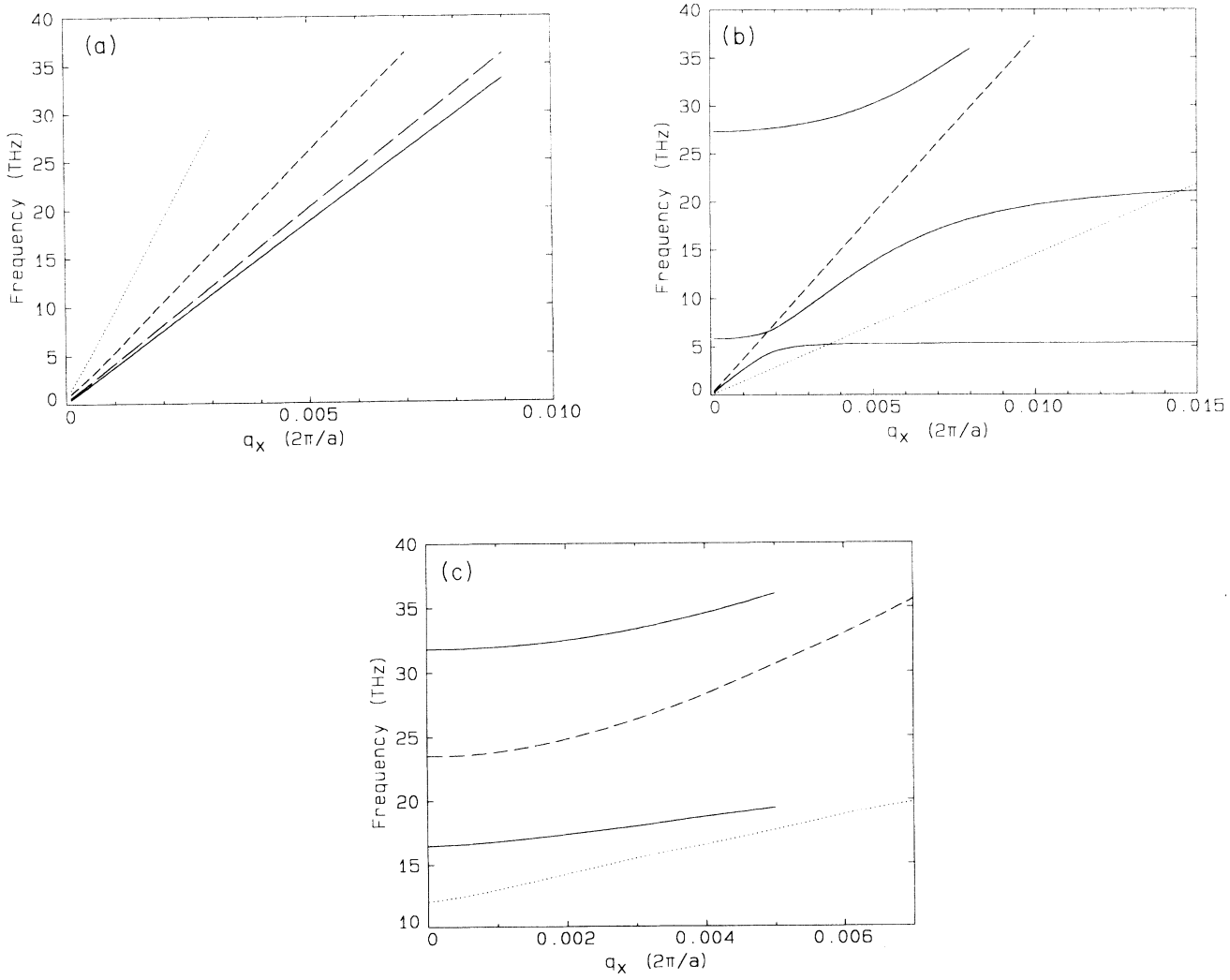

FIG. 3. (a) Acoustic plasmon dispersion for the two-dimensional band structure in the eleven-band tight-binding model along the $\mathbf{q}=(q_x,0,q_z)$ directions. The different line types indicate different values for q_z: $\cdots$ $q_z=0.25$; $-\,-\,-$ $q_z=0.5$; $-\cdot-\cdot-$ $q_z=0.75$; —— $q_z=1.0$. q_z is in units of $[(2\pi/c)]$. a and c are lattice constants. (b) Phonon-plasmon mixing for the acoustic plasmon of (a) for $\mathbf{q}=(q_x,0,2\pi/c)$. The different line types have the following meaning: $\cdots$ borderline for damping; $-\,-\,-$ uncoupled plasmon; —— coupled La_z^z-O_z^z phonon-plasmon modes near the Z point. (c) Phonon-plasmon mixing for the massive plasmon of model M1 taking interlayer coupling into account. $\mathbf{q}=(q_x,0,2\pi/c)$. $\cdots$ borderline for damping; $-\,-\,-$ uncoupled plasmon; —— coupled O_z phonon-plasmon modes near the Z point. Lower mode, phononlike; upper mode, plasmonlike.

mode. Finally, in a purely plasmon-dominated mechanism the isotope effect vanishes completely. Note in this context that the isotope effect is smallest for materials with the highest T_c's and becomes normal for very low T_c values.

In addition to the plasmon-induced variation of the isotope effect just discussed, the nonlocal character of the EPI found in our calculations means that there is a continuous distribution of "optimal lengths" for pairing in the neighborhood of the optimal length for pairing corresponding to the O_z^z frequency.[5] This implies a certain insensibility of pairing to the phonon frequency and thus a further reduction of the isotope effect can be expected.

IV. SUMMARY

Within a suitable microscopic model for the description of the electronic density response in the HTSC's, which has been extended to include dynamical screening, we find a strong increase of the already large nonlocal electron-phonon coupling strength as found in the adiabatic approximation when passing over to the nonadiabatic regime. The small dispersion of the electronic band structure in the c direction leads to strong mixing of low-lying plasmons and phonons of the same symmetry in the Λ direction and to an insulatorlike charge response within a certain tube (depending on the frequency) along this direction, while outside this tube and in particular in the (q_x,q_y) plane we have a metallic charge response. In particular for the plasmonlike mode very large changes of the crystal potential have been calculated Further, the possibility of an acoustic plasmon is investigated, which disappears if interlayer hopping is taken into account. Finally, a plasmon-induced variation of the oxygen isotope effect is outlined. Altogether, our calculations point to the coexistence of coupled phonons and plasmons of special type, around the Λ direction, with large coupling strength to the electrons. A possible resonance coupling between phonons and plasmons may well be triggered by a van Hove–like DOS peak. These findings could be useful on the route to understand the underlying mechanism for pairing in the HTSC's and their high T_c values.

ACKNOWLEDGMENTS

We thank Q. Chen for useful discussions. Financial support by the Deutsche Forschungsgemeinschaft is gratefully acknowledged.

[1]W. E. Pickett, Rev. Mod. Phys. **61**, 433 (1989).
[2]C. Falter, M. Klenner, and W. Ludwig, Phys. Lett. A **165**, 260 (1992).
[3]C. Falter, M. Klenner, and W. Ludwig, Phys. Rev. B **47**, 5390 (1993).
[4]C. Falter, M. Klenner, Q. Chen, and W. Ludwig, Solid State Commun. **88**, 87 (1993).
[5]C. Falter, M. Klenner, and Q. Chen, Phys. Rev. B **48**, 16 690 (1993).
[6]H. Krakauer, W. E. Pickett, and R. E. Cohen, Phys. Rev. B **47**, 1002 (1993).
[7]C. O. Rodriguez, A. I. Liechtenstein, I. I. Mazin, O. Jepsen, O. K. Andersen, and M. Methfessel, Phys. Rev. B **42**, 2692 (1990).
[8]T. Jarlborg, Phys. Lett. A **164**, 345 (1992).
[9]D. J. Singh, Physica C **212**, 228 (1993).
[10]R. G. Gordon and Y. S. Kim, J. Chem. Phys. **56**, 3122 (1972).
[11]R. E. Watson, Phys. Rev. **111**, 1108 (1958).
[12]F. Herman and S. Skillman, *Atomic Structure Calculations* (Prentice-Hall, Englewood Cliffs, NJ, 1963).
[13]J. P. Perdew and A. Zunger, Phys. Rev. B **23**, 5048 (1981).
[14]C. Falter, Phys. Rep. **164**, 1 (1988).
[15]V. Z. Kresin and H. Morawitz, Phys. Rev. B **37**, 7854 (1988).
[16]M. L. Cohen, in *Superconductivity,* edited by R. Parks (Dekker, New York, 1969), p. 615.
[17]Y. Takada, J. Phys. Soc. Jpn. **49**, 1267 (1980).